CONTROLLED VLF WAVE INJECTION EXPERIMENTS IN THE MAGNETOSPHERE

R. A. HELLIWELL
Radioscience Laboratory, Stanford University, Calif. 94305, U.S.A.

Abstract. Whistler-mode waves injected into the magnetosphere from ground sources (e.g., lightning discharge, vlf transmitters) are used to probe the distribution of ions and electrons in the magnetosphere. They also cause wave growth (vlf emissions) and precipitation of electrons. Bursts of X-rays (> 30 keV) and enhancements of D-region ionization are examples of precipitation effects caused by lightning-generated waves. Growing narrowband wave trains are triggered by manmade coherent waves. Growth rates of ~ 100 dB s^{-1} and total growths up to 30 dB have been measured using 5.5 kHz signals transmitted from Siple Station, Antarctica. Another source of coherent wave input to the magnetosphere are the harmonics from commercial power line systems. Power line harmonic radiation may suppress triggered emissions or change their frequency-time slope. Exponential growth of narrowband emissions is explained in terms of cyclotron resonance between the waves and trapped energetic electrons, with feedback included. Applications of wave injection experiments include: (1) study of emission mechanisms, (2) control of energetic particle precipitation, (3) diagnostics of cold and hot plasma, and (4) vlf communications.

Very low frequency whistler-mode waves interact strongly with the cold and hot charged particles of the magnetosphere. Because of the dispersion and anisotropy of the magnetosphere the distribution of the thermal electrons and ions can be found using vlf waves observed on the ground (Carpenter and Park, 1973) and within the

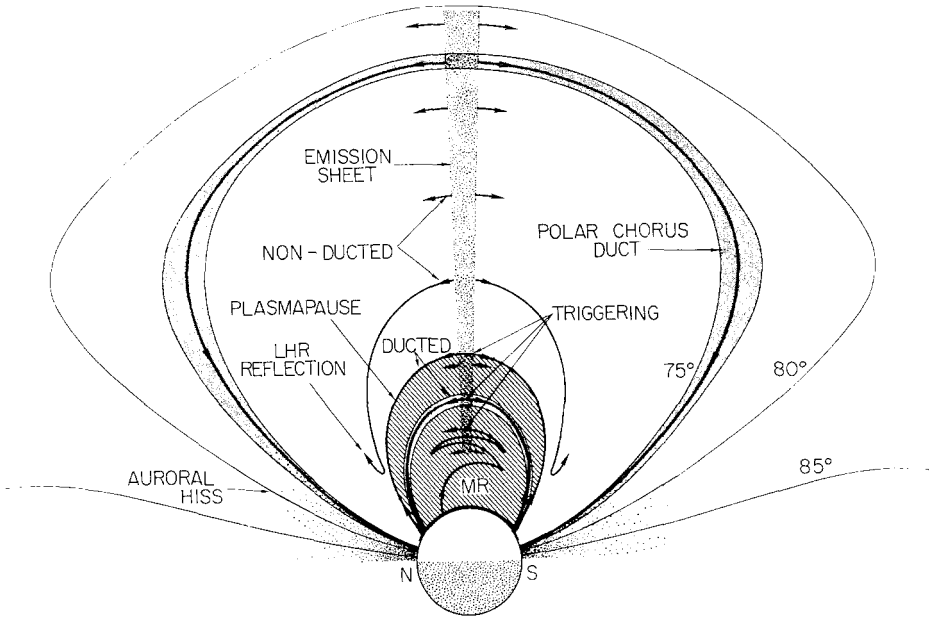

Fig. 1. Distribution of low-frequency waves in the geomagnetic meridional plane on the dayside of the Earth (after Helliwell, 1969).

Space Science Reviews **15** (1974) 781–802.

magnetosphere (Smith and Angerami, 1968; Edgar, 1972). The relation of whistler paths and vlf energy sources to the magnetosphere is sketched in Figure 1.

Energetic particles can exchange energy with the slow moving whistler waves through resonant interactions (Gendrin, 1972; Kimura, 1967). In cyclotron resonance involving electrons wave growth is accompanied by reduced pitch angles and correspondingly lowered mirror points. A self-sustaining cyclotron interaction can be triggered by injecting vlf waves from the ground. Results include the emission of strong radio signals (up to 30 dB above the level of the triggering signal) and the precipitation of the resonant particles into the ionosphere. Applications of vlf triggering include: (1) study of mechanism of emission of radio waves from planetary magnetosphere, (2) control of precipitation for the purpose of modifying the ionosphere, (3) remote sensing of the characteristics of hot and cold particle populations, and (4) new vlf communications techniques.

The purpose of this paper is to review briefly the results and interpretation of vlf wave injection experiments, emphasizing resonant particle interactions. Topics will be presented in roughly chronological order and include: (1) cold plasma diagnostics, (2) triggered emissions, (3) triggered precipitation, (4) cyclotron oscillator theory, and (5) controlled vlf wave injection experiments.

1. Cold Plasma Diagnostics

The cold plasma electron density is monitored using whistlers of the type shown in Figure 2a. Each of the parabola-shaped traces in the upper and lower panels corresponds to a particular field-aligned duct within the plasmasphere, shown in Figure 1. The point of minimum time delay, or 'nose', on each trace measures the minimum gyrofrequency f_{Ho} along the path. For a given model of the Earth's field f_{Ho} defines the path latitude. The time delay to the nose measured from the originating atmospheric at $t=0$ depends upon the integrated group delay over the path and hence is a measure of the electron density. By assuming a model for the electron density distribution along a field line, each delay can be converted to an equatorial electron density at the corresponding altitude. The electron density in the magnetosphere shows diurnal and seasonal variations and in addition shows a marked dependence upon substorm phase. These results are discussed elsewhere (Carpenter and Park, 1973).

2. Triggered Emissions

Whistlers that provide the diagnostic data may also trigger narrowband emissions, as shown in the lower panel of Figure 2a. In this case there are five emissions, each of which begins at the upper cutoff frequency ($\sim f_{Ho}/2$) of a different whistler trace. Whistler stimulated emissions (WSE's) are believed to be caused by a cyclotron instability and are one of the main objects of study in the controlled vlf wave injection experiments. Rising emissions triggered by the Morse dashes from NAA (10^6 W output) on 14.7 kHz are also seen in the upper panel of Figure 2a. These are called

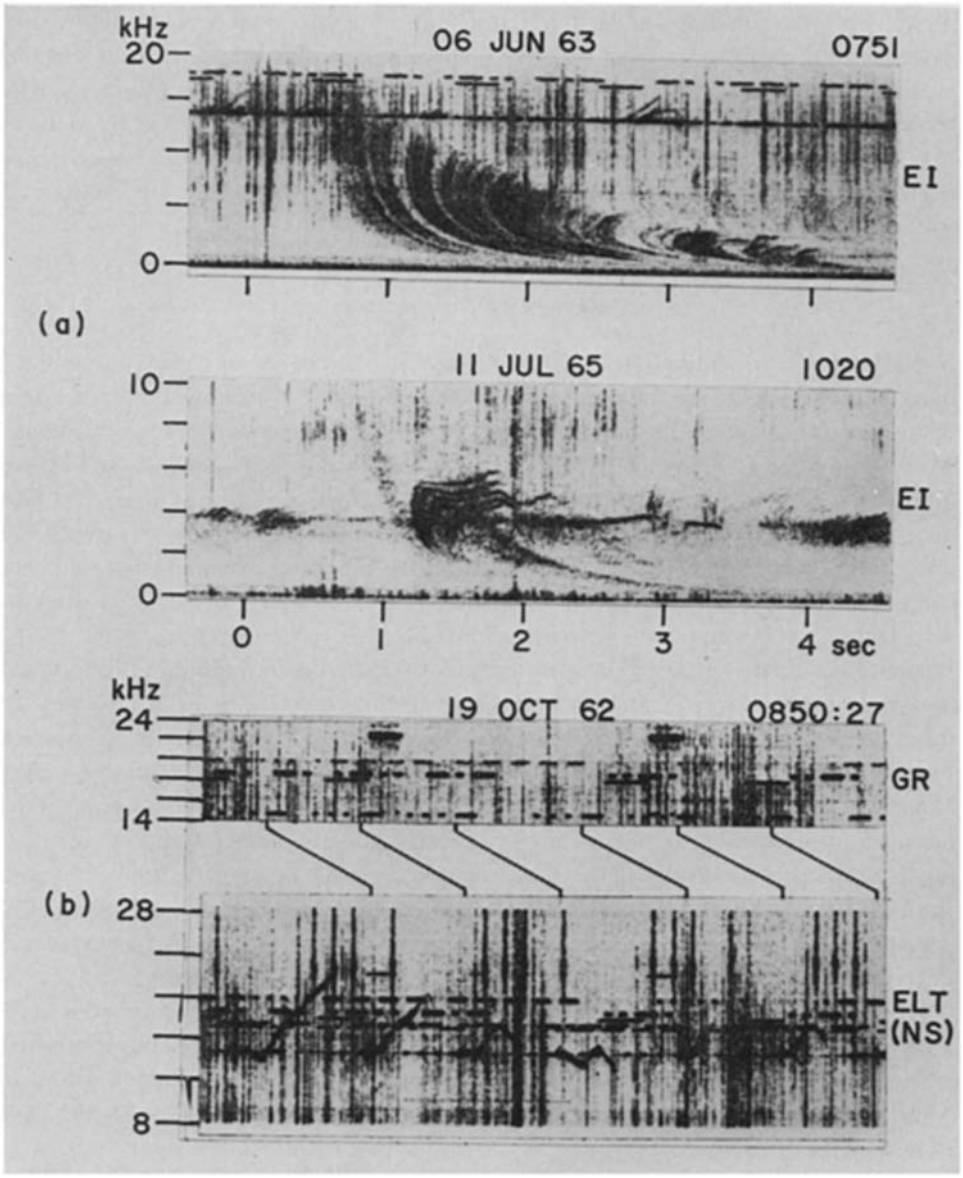

Fig. 2. (a) Nose whistlers; (b) ASE's from NAA on 14.7 kHz (after Helliwell, 1969).

artificially stimulated emissions (ASE's). Better examples of ASE's are shown in Figure 2b. The Morse dot-dash pattern as transmitted from NAA at Cutler, Maine, and observed at Green Bank, West Virginia, is shown in the upper panel. The lower panel of Figure 2b shows the signals as received near the conjugate point on the research ship ELTANIN. The slanting lines between the two panels connect each transmitted dash with its corresponding emission. Their time displacement of 0.8 s is ap-

proximately the one-hop travel time from transmitter to receiver. Only the Morse dashes produce emissions. Each triggered emission is characterized by an initial rise in frequency which may continue or may be followed by a decrease in frequency. The record also shows apparent changes in slope of the triggered emissions at frequencies of other vlf stations. This point will be discussed later in connection with the new controlled experiments. Triggered emissions have also been observed on Omega vlf stations operating at only 100 W output (Kimura, 1968).

3. Triggered Precipitation

In addition to stimulating narrowband emissions, whistler-mode signals dump electrons into the ionosphere. In a recent experiment bursts of X-rays were observed in a balloon at 30 km altitude at the same time that whistler-triggered risers were observed on the ground below (Rosenberg *et al.*, 1971). An example of this association is shown in Figure 3. The bursts of noise on the vlf channel show a one-to-one correlation with the X-ray bursts in the upper panel. With the aid of conjugate-point recordings the noise bursts were found to have been triggered by whistlers originating in northern hemisphere lightning discharges. The whistlers themselves were usually too weak to be detected even though their triggered emissions were quite strong.

In another related experiment whistlers are associated with a temporary modification of the nighttime D-region ionization level (Helliwell *et al.*, 1973). An example of the effect is shown in Figure 4. The signal strength of NSS observed at Eights Station (lower panel) was increased about 6 dB at the time of arrival of the whistler (upper panel). On other occasions the signal was depressed rather than enhanced. The sign of the perturbation depends on frequency and on the orientation of the receiving loop, suggesting that the cause is a change in the phase relations between different waveguide modes. Both positive and negative perturbations show similar recovery times, averaging 30 s.

Both the X-ray bursts and the vlf propagation perturbation have been interpreted in terms of resonant interaction between the waves and energetic electrons. A model of the interaction is shown in Figure 5. Electrons traveling opposite to the wave see a Doppler-shifted wave frequency equal to their own gyrofrequency. Thus a whistler or an emission traveling southward interacts with electrons traveling northward. These electrons are pitch-angle scattered after interacting with the wave. Some have their mirror points lowered resulting in some precipitation in the northern hemisphere and some in the southern hemisphere. In the X-ray experiment the wave bursts arrived ahead of the X-ray bursts by 0.3–0.4 s. This time difference was explained using the model shown in Figure 5. The wave packet travels at group velocity over a $\frac{1}{2}$ hop path whereas the particles travel at their parallel velocity over a $\frac{3}{2}$ hop path.

Using whistler measurements the energies of the resonant electrons in these two experiments have been calculated. Curves of the electron energy vs frequency are shown in Figure 6. In both experiments the observed wave frequencies correspond to electron energies (>30 keV) that are capable of penetrating the D-region ($h<90$ km) and causing X-rays and ionization.

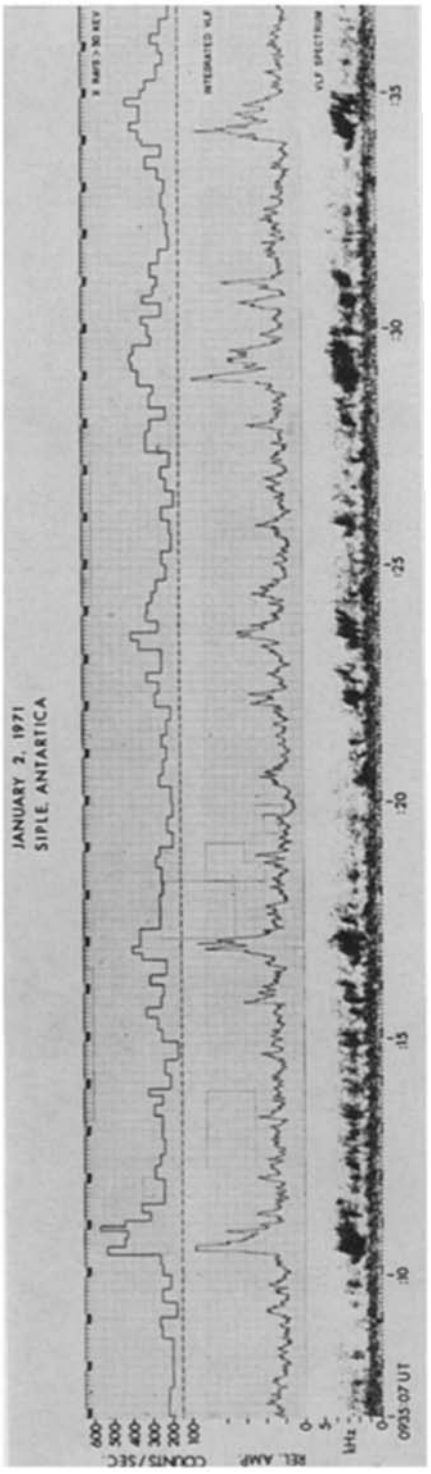

Fig. 3. A 30-s segment of simultaneous recordings of X-ray count rate for $E > 30$ keV (top), integrated vlf amplitude from 0.6 to 5 kHz (middle), and vlf spectrum from 0 to 5 kHz (bottom), at Siple Station, Antarctica, on January 2, 1971. The dashed line in the top portion of the figure refers to the cosmic-ray background level of ~ 175 c s^{-1}. (Because of a plotting error the X-ray record must be shifted 0.15 s to the right relative to the vlf records.) (after Rosenberg *et al.*, 1971)

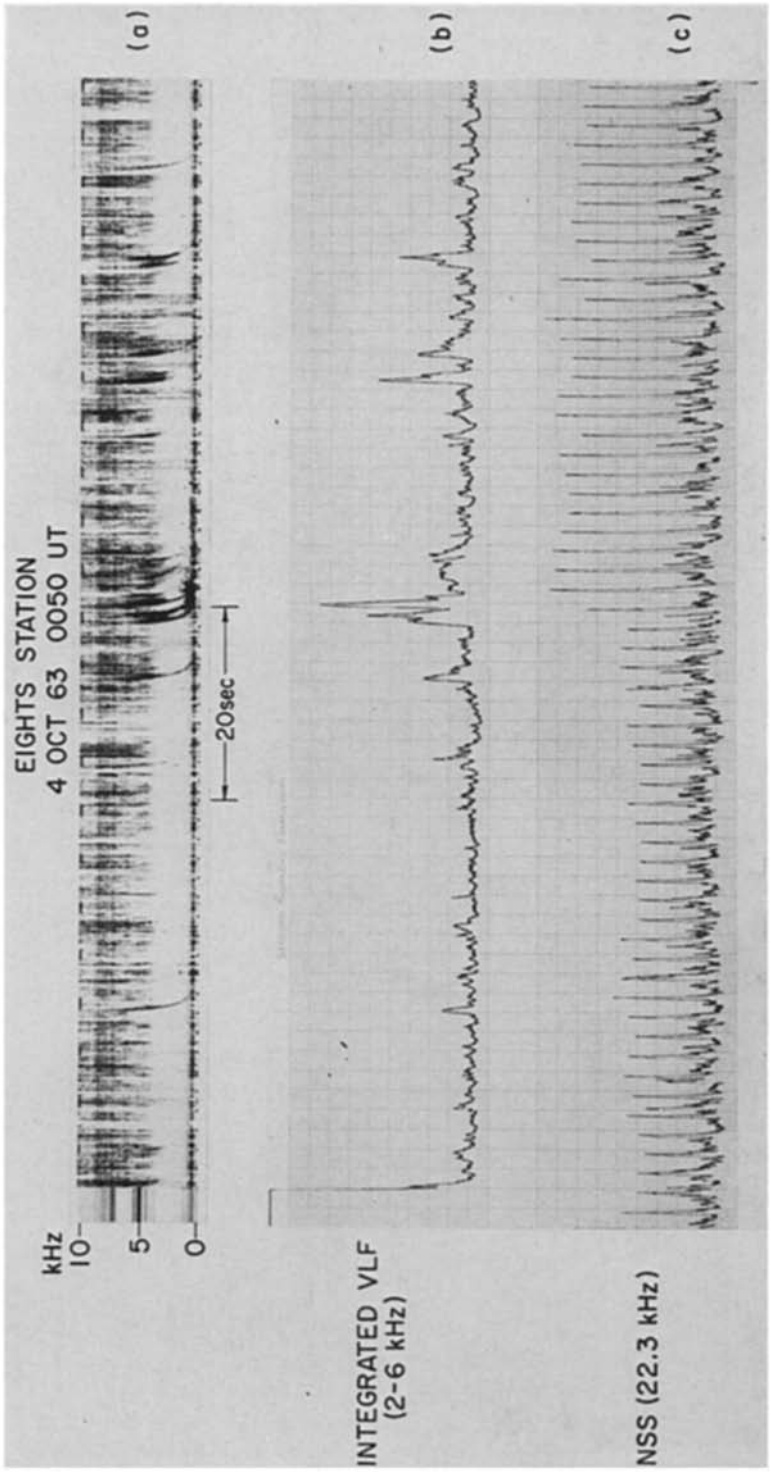

Fig. 4. (a) Whistler spectra; (b) whistler amplitude, 2–6 kHz; and (c) NSS pulse transmissions, observed at Eights Station (after Helliwell *et al.*, 1973).

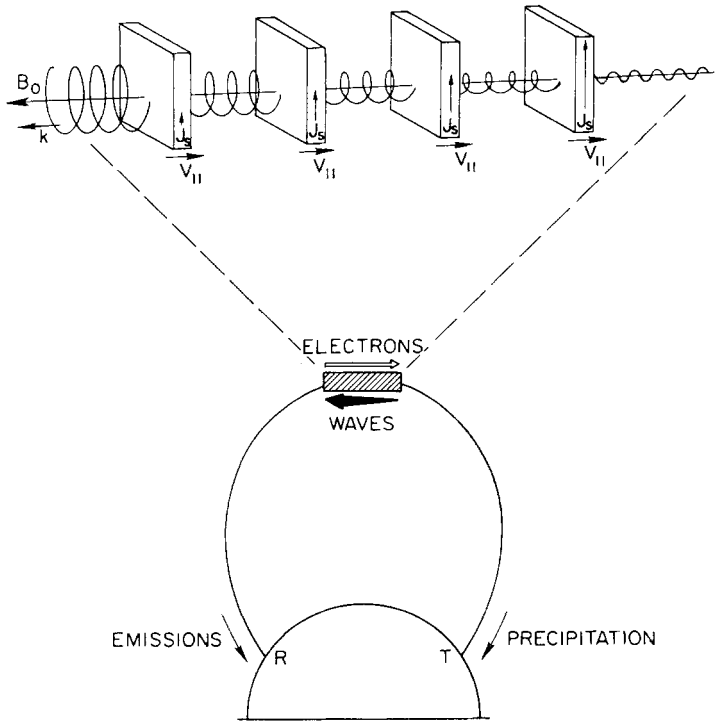

Fig. 5. Sketch of interaction region model. Circularly-polarized waves transmitted from T resonate with oppositely traveling electrons near the equator. The train of electron sheets represents a continuous stream of resonant electrons. The resonant electrons in each sheet are phase-bunched by the wave, producing a transverse stimulated current, J_s. The change in wave amplitude shown across each sheet results from the addition of the wave component generated by J_s. Emissions travel to R while scattered electrons are precipitated at T (after Helliwell and Crystal, 1973).

4. Cyclotron Oscillator Theory

In view of the agreement between the cyclotron resonance interaction model and the observations it is worthwhile to develop the model further. A unique feature of the interaction is the narrowband, variable frequency character of the wave train, whether it be a whistler or a triggered emission. In addition other data have shown that the oscillation may continue for a time long compared with the bounce time of wave packets over the path (Brice, 1964). Thus some kind of long enduring feedback oscillalation is required to explain the results.

In the upper part of Figure 5 is sketched a model which has been used to predict the effects of feedback in the cyclotron resonance interaction (Helliwell and Crystal, 1973). The electron stream is assumed to be represented by equally spaced infinite sheets of spiralling electrons that are traveling to the right at the parallel resonant velocity $v_{\|}$. The right-hand circularly-polarized waves travel to the left and are excited by the transverse current in each sheet. These currents are created by phase-bunching of the electrons as they interact with the magnetic field in preceding portions of the

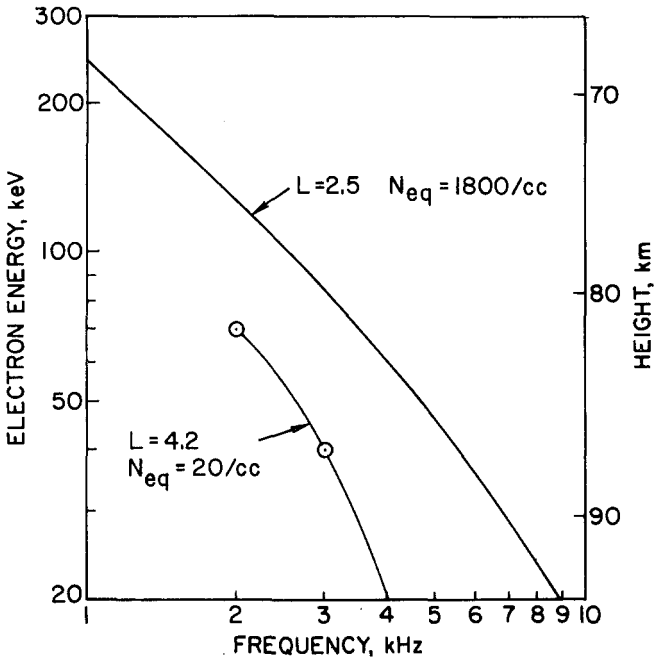

Fig. 6. Relation between electron energy (and corresponding height of penetration) and whistler frequency for $L = 2.5$, $N_{eq} = 1800$ cc^{-1} (after Helliwell *et al.*, 1973) and for $L = 4.2$, $N_{eq} = 20$ cc^{-1} (replotted from Rosenberg *et al.*, 1971).

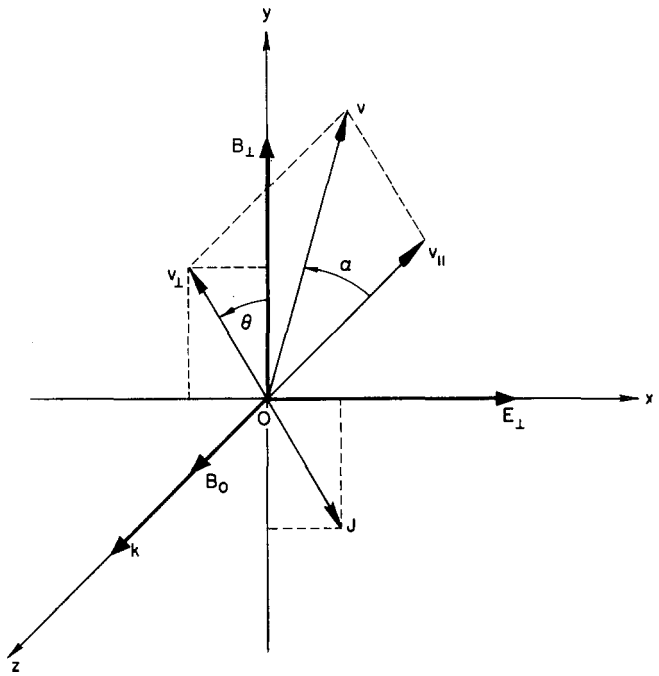

Fig. 7. Coordinate system and relation of wave fields and electron velocities (after Helliwell and Crystal, 1973).

wave train. In the case shown, the whistler mode waves grow continuously from the input on the right to the output on the left. The length of the interaction is of the order of 1000 km and is derived from consideration of the inhomogeneity in the magnetosphere (Helliwell, 1967).

Calculations based on the physical model of Figure 5 start from the description of the parameters given in Figure 7. The $E_\perp$ and $B_\perp$ of the wave are mutually perpendicular and the wave travels in the $+z$ direction. The resonating particles travel in the $-z$ direction with parallel velocity $v_\parallel$ and perpendicular velocity $v_\perp$. The perpendicular velocity $\bar{v}_\perp$ of a resonant electron makes an initial angle θ with $\bar{B}_\perp$. In the absence of interaction with the wave the resonance condition would require that θ remain constant throughout the interaction. Associated with the perpendicular velocity is a transverse

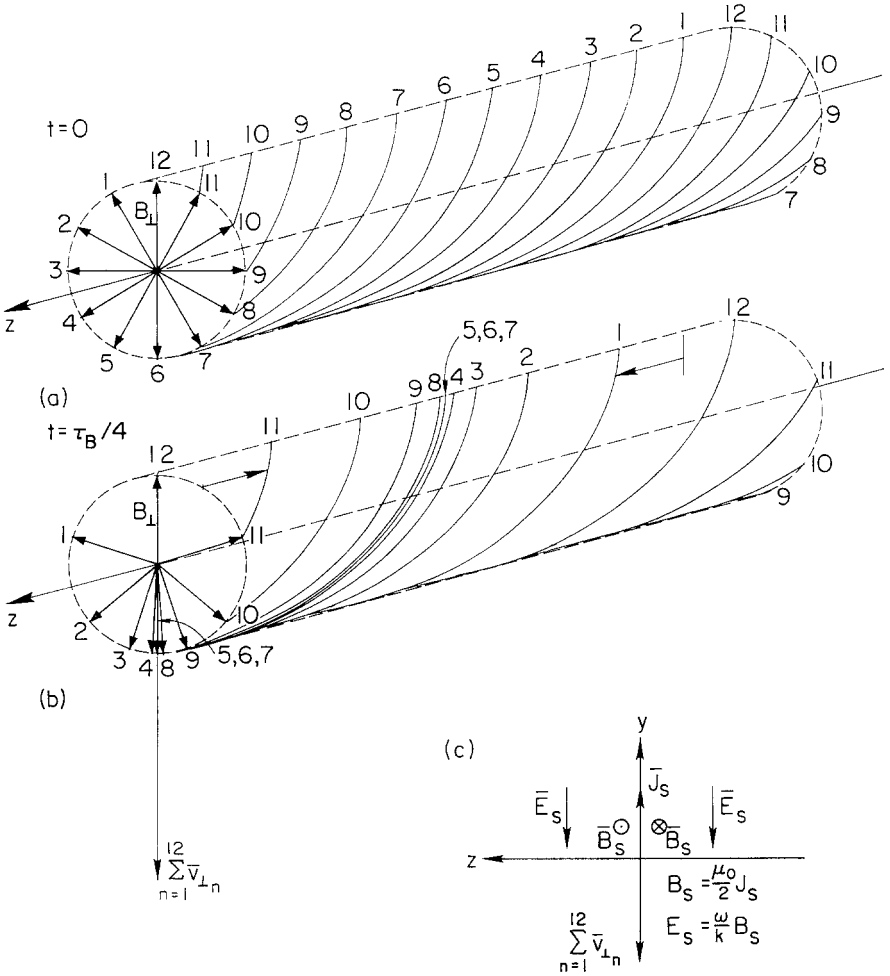

Fig. 8. Helical loci of the perpendicular velocities of twelve elementary streams: (a) before bunching; (b) after some bunching. $B_\perp$ is represented by vector #12. (c) ensemble sheet current J_s and associated induced magnetic (B_s) and electric (E_s) fields (after Helliwell and Crystal, 1973).

current $\bar{J}$ which is in the opposite direction because of the negative charge of the electron. It is this current $\bar{J}$ which can be visualized as providing the source for a stimulated electromagnetic wave.

To fully represent the possible phase angles between the perpendicular velocities and the magnetic field of the wave the model in Figure 8 is constructed. Initially it is assumed that the electrons are randomly phased with respect to the wave so that to first order there is no significant perpendicular current. To represent this situation 12 test electrons equally spaced in phase with respect to $B_\perp$ are assumed. These are shown in the diagram of Figure 8a. It is further assumed that the stream is broken up into 12 helices which wrap around the cylinder shown in the diagram. After these helical distributions of electrons have passed through the wave the $qv_\perp \times B_\perp$ force exerted by the wave causes the helices to drift forward and backward along the z axis, with the result that there is bunching of the helices as shown in Figure 8b. By taking a section of this cylinder and adding up the velocity vectors it is seen that a net velocity is obtained as compared with zero velocity in Figure 8a. When this velocity is multiplied by the electron density and the charge the transverse current is obtained. This transverse current is called J_s and, as shown in Figure 8c, creates field components on the forward and backward sides of the sheet, labeled B_s and E_s.

The phase-bunched current launches waves in both directions just as a current

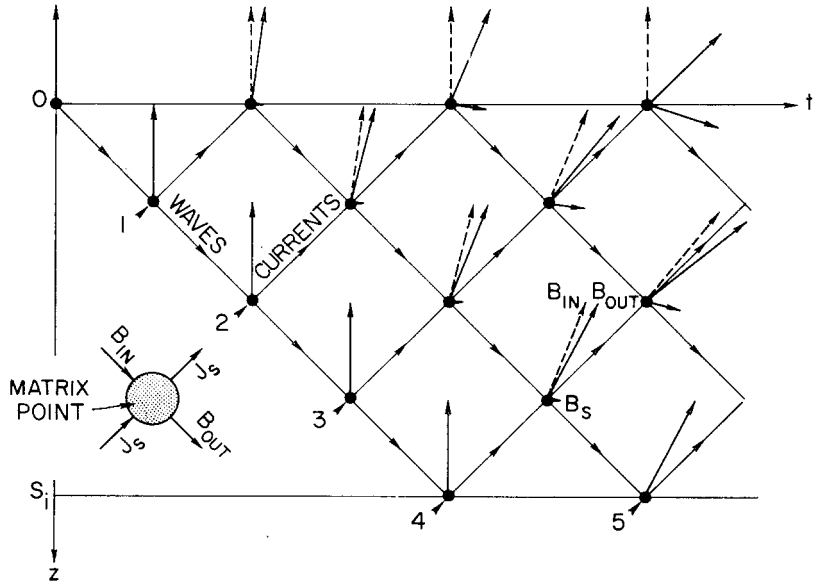

Fig. 9. Schematic space-time matrix showing how stimulated wave fields are added to the total field. The loci of the waves are given by the diagonals slanting downward to the right. The loci of the ensemble currents sheets, numbered 1 through 5, are given by the diagonals slanting upward to the right. The inset diagram shows a typical matrix point, at which the stimulated field B_s is added, vectorially, to the incoming total field B_{in} to produce the outgoing field B_{out}. This value of B_{out} is applied to the sheet current J_s as it moves to the next matrix point. At each matrix point the magnetic field vector of the incoming wave is shown by a dashed line (after Helliwell and Crystal, 1973).

generator would launch waves on an infinite transmission line. However because of the phasing only the waves traveling to the left add up to a significant result, as in an endfire array of antennas. This is the source of the stimulated radiation. It is clear that the stimulated radiation must be added to the applied signal to obtain the total field at any sheet of electrons.

The effect of including feedback between the electrons and the waves is illustrated on the space-time diagram of Figure 9. The solid vectors represent the total field at any given point in space and time. The wave front is represented by the line sloping downward to the right and the current sheets by the lines labeled 1, 2, 3, 4 and 5, sloping upward to the right. At each matrix point the field (short solid vector) generated by the phase bunched current is vectorially added to the incoming field (dashed vector) from the upper left to give the total field. It can be seen that the total field shows changes in phase and in magnitude as a result of the feedback process.

An example of the space-time variation of the total field for a particular numerical case is shown in Figure 10. The contours are lines of constant intensity with the solid lines corresponding to intensities greater than the input signal and the dashed lines to intensities less than the input signal. The output signal is seen to vary cyclically like

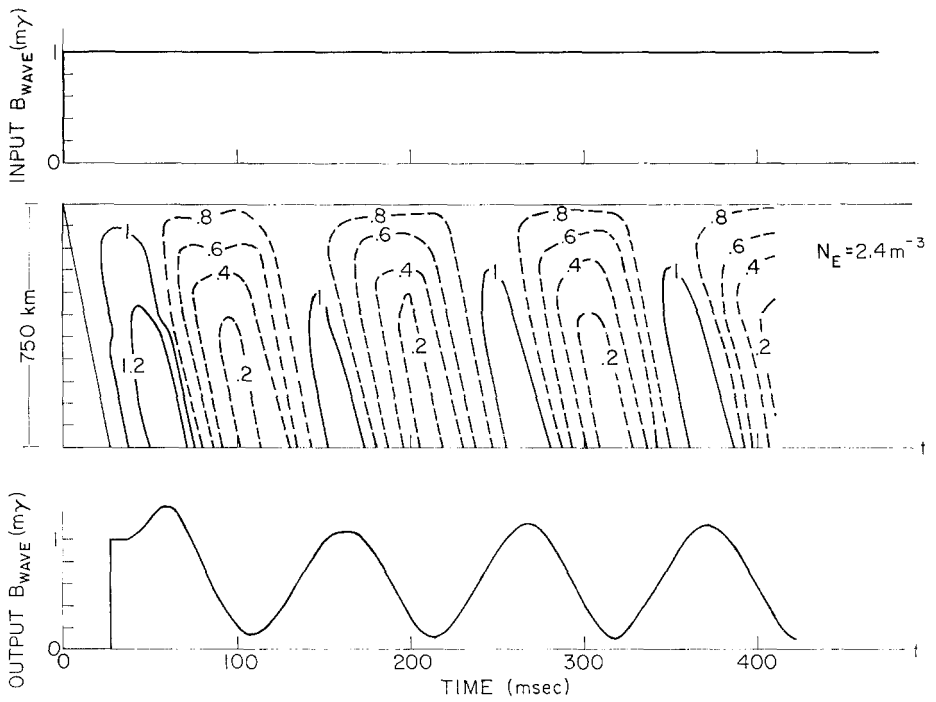

Fig. 10. Middle panel shows space-time matrix of total $B_\perp$ field computed for a continuous triggering signal of 1 mγ and a stream density of 2.4 m^{-3}. Contours show loci of constant total intensity. Solid contours represent total field magnitudes greater than the input field and dashed contours represent reduced magnitudes. The time variations of input and output fields are shown in the upper and lower panels, respectively (after Helliwell and Crystal, 1973).

the beat between two constant-amplitude waves. In fact the curve of the output signal can be very nearly reproduced by adding two sine waves about 9 Hz apart in frequency. The model thus predicts strong pulsations when the stimulated radiation is comparable in magnitude to the applied signal. The similarity between this prediction and some experimental results is shown in Figure 11.

The growth rate of the process described above is best illustrated by the application of a short pulse which starts the feedback process. The oscillation then becomes self-sustaining, growing exponentially with time until saturation is reached. The curves of Figure 12 show on a log plot the theoretical response of the system to short exciting pulses. The nature of the exciting pulse is not particularly important as long as it doesn't

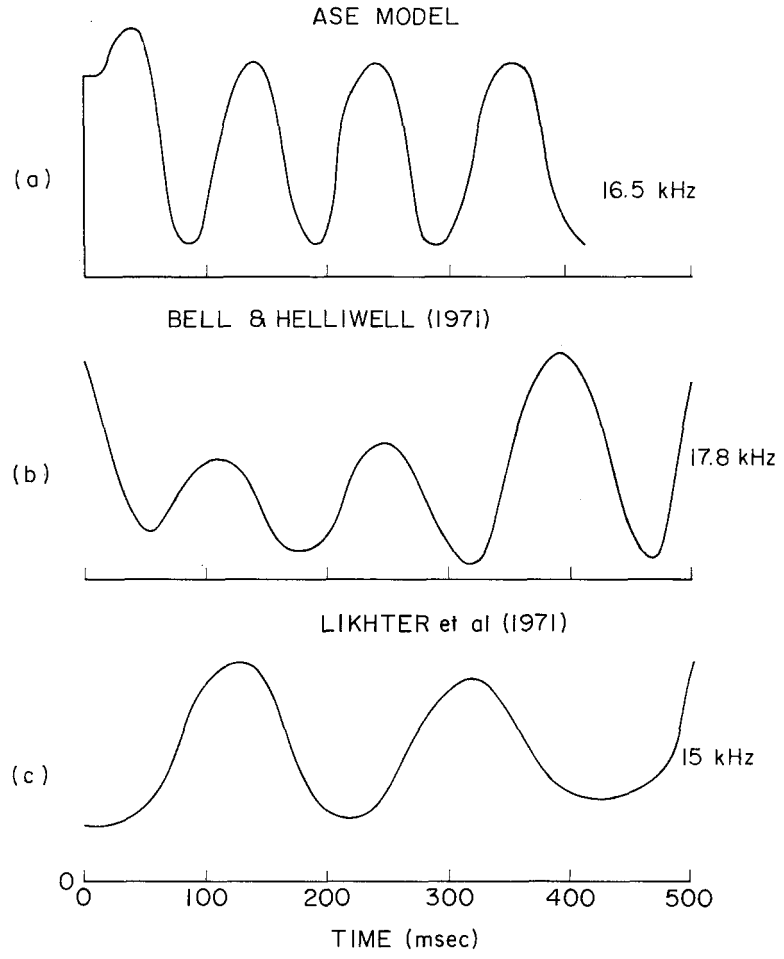

Fig. 11. (a) Initial part of theoretical pulsation replotted from Figure 10. (b) Portion of observed natural pulsations from NAA on 17.8 kHz (Bell and Helliwell, 1971). (c) Replot of envelope of pulsating whistler-mode signal observed from Russian transmitter on 15 kHz (Likhter *et al.*, 1971) (after Helliwell and Crystal, 1973).

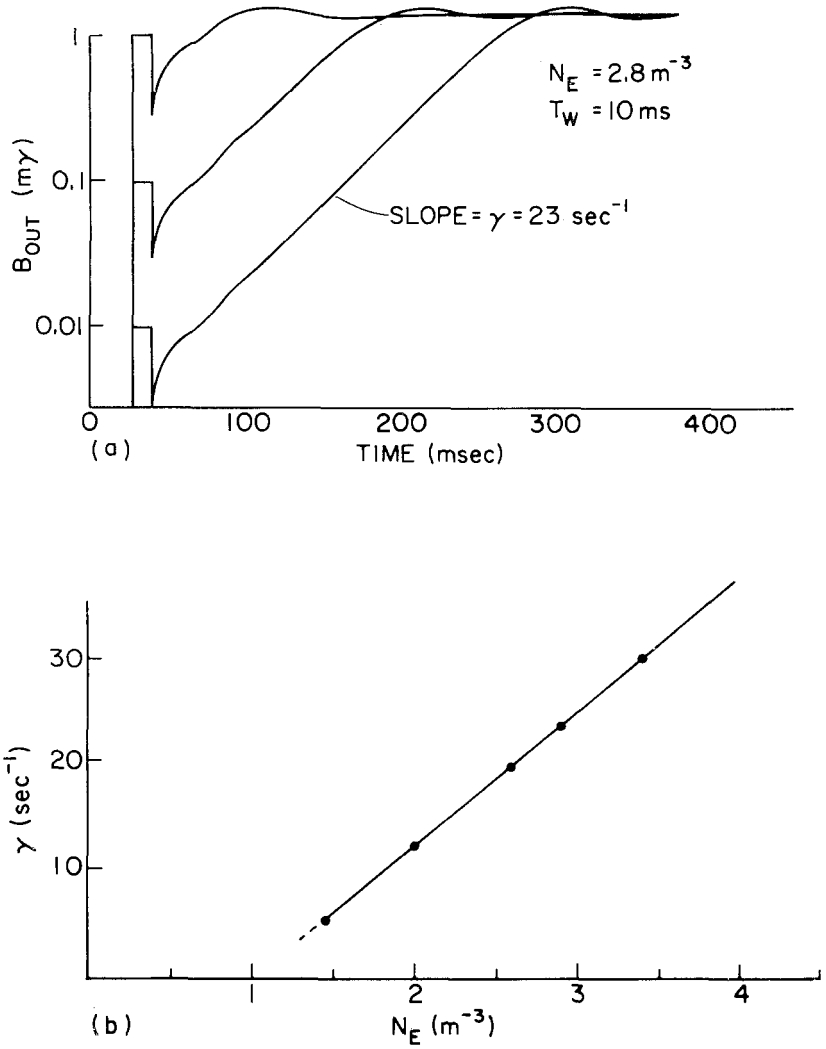

Fig. 12. (a) Logarithm of the output field vs time for 10 ms pulse of variable amplitude (1 mγ, 0.1 mγ, 0.01 mγ) and a stream density of 2.8 m^{-3}. An exponential growth rate of $\gamma = 23\ s^{-1}$ is indicated by the straight line segments of the curves. (b) Variation of the exponential growth rate, shown in (a), with stream density. Growth rate is zero below the threshold density of 1.5 m^{-3} (after Helliwell and Crystal, 1973).

interfere significantly with the stimulated emission. It is seen that the growth is purely exponential until the output nears saturation. The growth rate is linearly proportional to the stream density in this model. These results suggest that if the triggering signal is sufficiently weak there may be an appreciable delay in the initial appearance of the emission. Such a delay has been observed experimentally (Helliwell and Crystal, 1973).

Shortly after reaching saturation the oscillation enters the steady state, in which there are no variations in the envelope of the current or field with time at any given

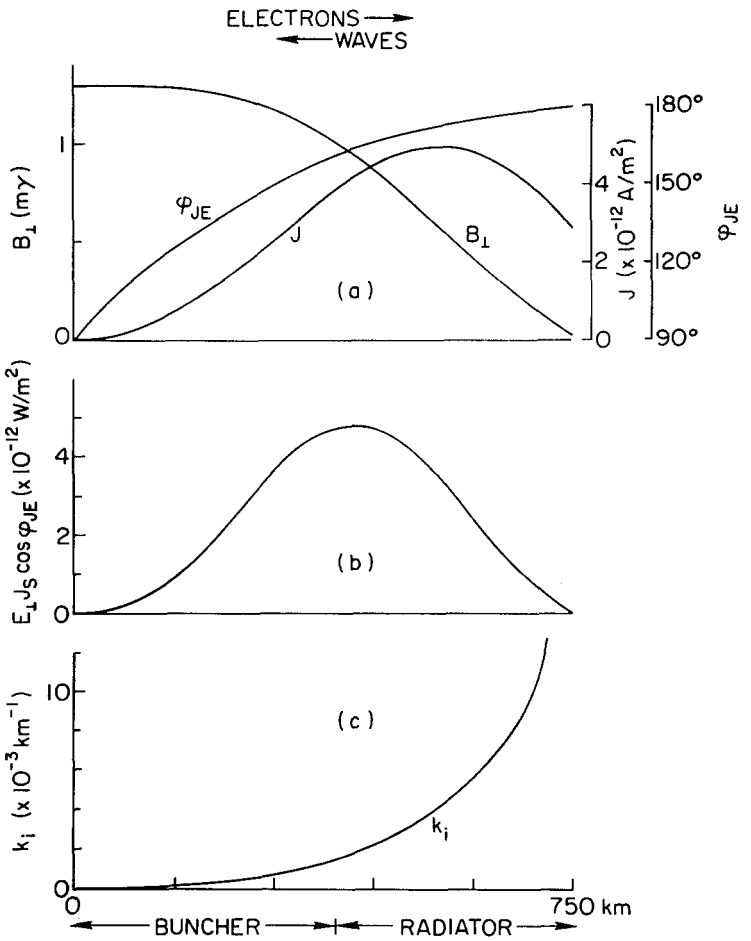

Fig. 13. (a) Steady-state spatial variations of $B_\perp$, J_s and ϕ_{JE} for self-excited oscillations, with $N_E = 2.8$ m^{-3}. (b) Power density generated by phase-bunched electrons. (c) Growth rate k_i computed from (a) (after Helliwell and Crystal, 1973).

location. The spatial variations of the system parameters for such a case are illustrated in Figure 13a, which shows $B_\perp$, $J_\perp$ and the phase angle ϕ_{JE} between $\bar{J}$ and $\bar{E}$ as a function of distance. The generated power is given by $E_\perp J_s \cos\phi_{JE}$ and varies as shown in Figure 13b. It is seen that maximum power generation occurs near the middle of the interaction region. If one were to describe a spatial growth rate for the total field then it could be represented by the curve shown in Figure 13c. The growth rate becomes infinite at the input to the interaction region. It is noted that in this case there is no triggering signal at the input and the behavior is like that of an oscillator. It is further noted that even though the medium is basically inhomogeneous the existence of a steady state implies zero bandwidth in the output.

From the experimental and theoretical work already reviewed it is clear that more controlled experiments are required to advance our understanding of wave particle

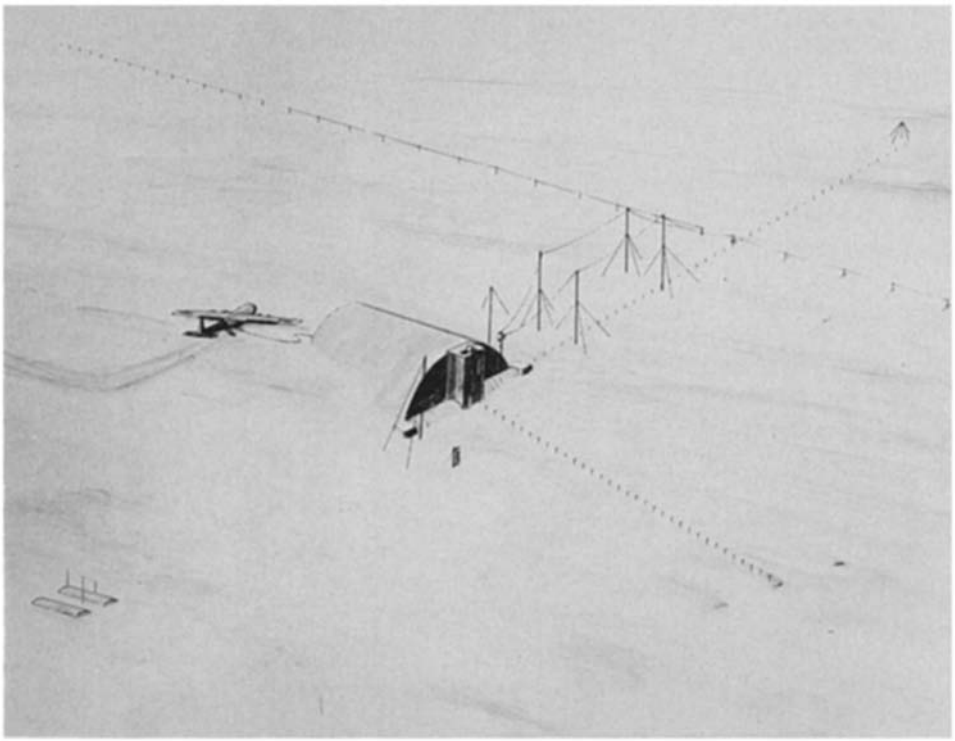

Fig. 14. Artist's sketch of Siple Station (after Helliwell and Katsufrakis, 1974).

interactions. For this purpose a new transmitting facility has just been established at Siple Station, Antarctica. Figure 14 shows an artist's sketch of this station. The building houses a 100 kW transmitter that drives a 21.3 km long balanced dipole. The dipole is supported 10–15 ft above the ice and resonates at 5.1 kHz. The location of the station was chosen to satisfy a number of criteria. First it was desired to be near the average position of the plasmapause at $L=4$. It was also necessary to locate the station over a thick ice cap in order to obtain a sufficiently high antenna efficiency. To observe the effects produced by the transmitter a receiving station was set up at the conjugate point at Roberval, Quebec. Satellites carrying vlf receivers track the Siple signals within the magnetosphere.

Some test results using the transmitter have been obtained from the receiving station at Roberval and are illustrated by the variable pulse length experiment in Figure 15 (Helliwell and Katsufrakis, 1974). In this experiment the power output of the transmitter was held constant. The frequency of radiation was switched between 5.0 and 5.5 kHz. In the case shown very little activity appears on the lower frequency although a few pulses and triggered emissions can be seen. Most of the activity is confined to 5.5 kHz. The pulse length was varied between 50 and 400 ms in 50 ms steps. The pulses were spaced by an interval equal to their length. Five pulses were transmitted at each pulse length.

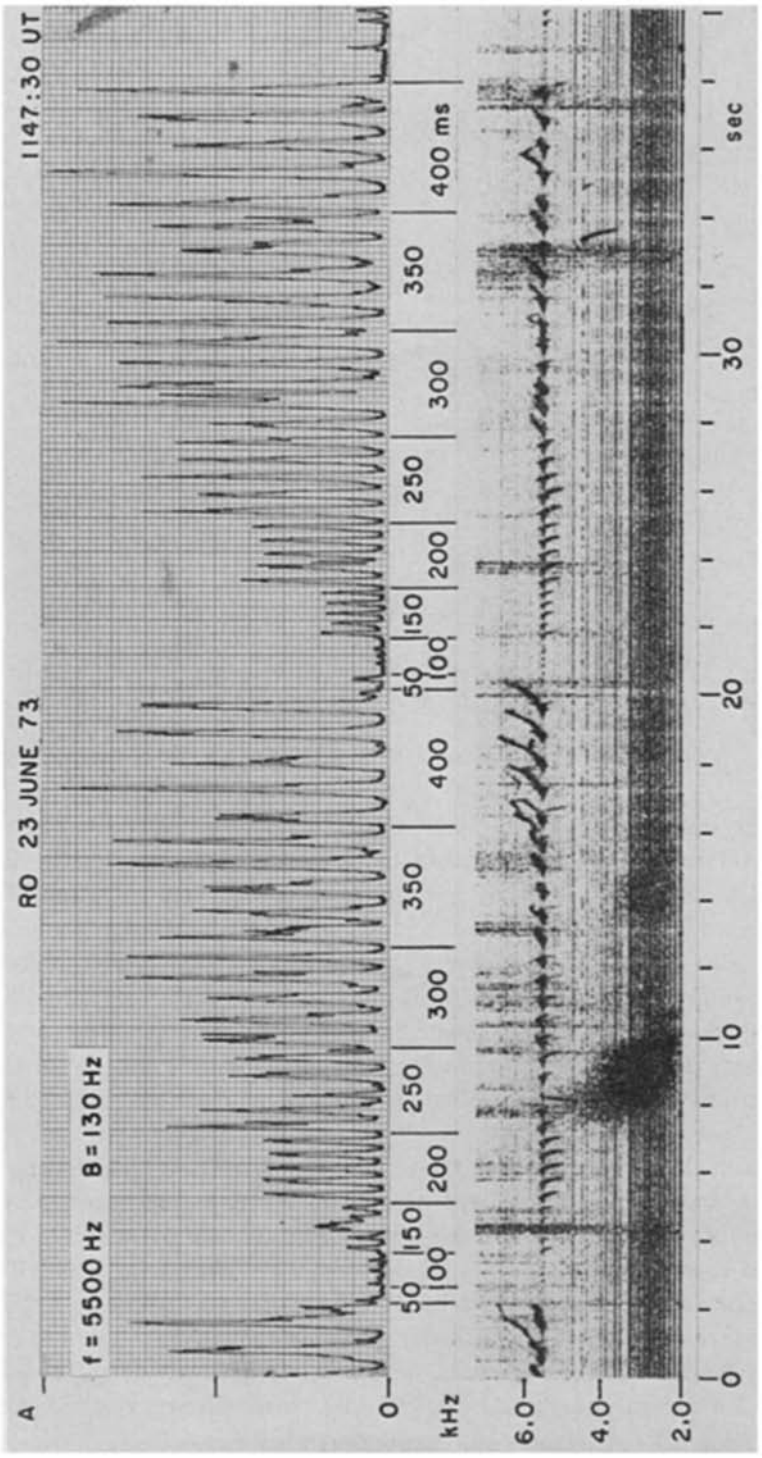

Fig. 15. Variable pulse length sequence received at Roberval. Lower panel shows the spectrum and upper panel the amplitude in a 130 Hz bandwidth centered on 5500 Hz. Pulse lengths vary from 50 ms to 400 ms in 50 ms steps as indicated by the numbers between panels. A two-hop whistler, with echoes at ~ 3 kHz, appears at 8–10 s, and originates in the sferic at 4.2 s. A strong well-defined two-hop whistler component is seen at about 8.2 s and corresponds to the one-hop delay of the Siple pulses (after Helliwell and Katsufrakis, 1974).

The short pulses, of 50 and 100 ms duration, produced extremely weak signals at the conjugate point. As the pulse length increased the intensity of the signal increased along with the intensity of the emissions. Initially the triggered emissions were falling tones. They actually began with a slight rise in frequency then quickly turned over and fell in frequency. When the pulse length was changed from 250 to 300 ms the falling tone part of the emission was cut off and the emission appeared as a blob with no particular shape. With further increase in pulse length the emission became an irregularly rising tone. This behavior, beginning with weak falling tones and ending with strong rising tones, has been commonly found in the variable pulse length experiments conducted so far.

In the upper part of Figure 15 is shown the amplitude as a function of time in a 130 Hz band centered on 5.5 kHz. For the shorter pulses the peak intensity of the signal increases by a factor of two for each 50 ms increase in pulse length. Then as the pulse duration passes 300 ms the amplitude ceases to increase uniformly, showing some fading. Some of this fading is connected with the variation in the frequency of the triggered emission which moves in and out of the pass band of the filter.

Other signals have been found to interfere with the growth process illustrated above. Whistlers at the frequency of the transmitter can reduce the output of the amplified signal. An example is shown at about 9 s on Figure 15, in which a whistler trace is observed to suppress the next 250 ms pulse. This effect is observed with emissions as well as whistlers.

In view of the systematic increase in the peak intensity of the amplified pulses as a function of their length it is important to know how each individual pulse grows with time. This effect is illustrated in Figure 16, which is an expanded version of a portion of Figure 15 and which shows the individual behavior of the 150, 200 and 250 ms pulses. At the bottom of the figure are solid bars corresponding to the pulse input to the magnetospheric interaction region. The whistler mode delay has been subtracted so that the input pulse can be compared directly with the observed output. It is seen that the observed output reached a minimum very close to the leading edge of the applied signal. The slight hangover from previous emissions accounts for the fact that the output signal is not at its minimum value at the start of the input pulse. Following the minimum, the intensity of the amplified echo increases exponentially with time until the end of the pulse is reached. At that point the curve may flatten out or show considerable irregularity. It has been found that for longer pulses the growth will stop before the end of the pulse, indicating that a saturation level has been reached.

To show the detailed nature of the growth process records like that in Figure 16 were scaled for the pulse lengths of 150, 200, 250 and 400 ms. The 300 and 350 ms pulse lengths were omitted because their intensities were modified by emissions triggered by previous pulses. By plotting the log of the average intensities of these pulses with respect to the leading edge of each pulse we get a growth rate of 128 dB s^{-1} as shown in Figure 17. Different growth rates are found at other times, with values ranging from 30 dB s^{-1} to 200 dB s^{-1}. Because of the noise on the records it has not been possible accurately to measure the unamplified input signal but it is esti-

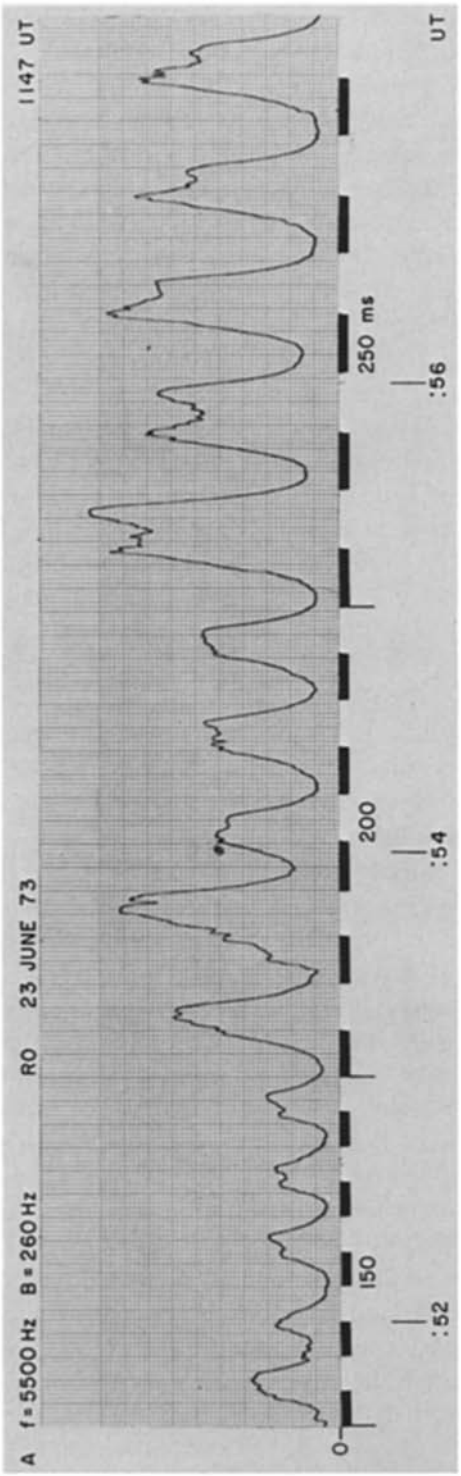

Fig. 16. Pulse envelope for the 150, 200 and 250 ms pulses of the second 18-s sequence shown in Figure 2. Solid bars represent the transmitted pulses corrected in time for the one-hop travel time of 2.02 s (after Helliwell and Katsufrakis, 1974).

mated to be at the point labeled A_i on Figure 17. The total gain or growth is then about 30 dB.

An important result of these experiments is a demonstration, given in Figure 17, that the interaction produces growth in time rather than in space. This result contrasts with theories (e.g. Liemohn (1967)) predicting spatial growth of the traveling waves, as in an amplifier in which all parts of the signal grow at the same rate as the wave travels through the medium. The present experimental results show on the contrary that the interaction resembles that of a phase-locked oscillator. The input signal is not amplified but turns on an oscillator whose output grows exponentially with time. The input signal appears to exercise phase control over the oscillation so that the growth can be

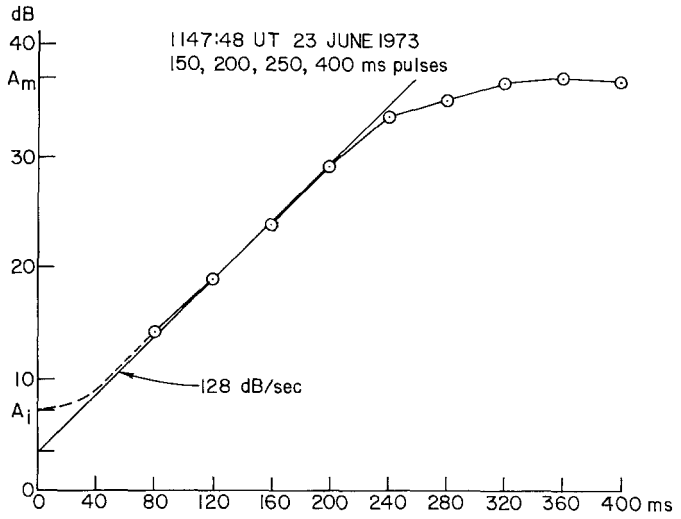

Fig. 17. Average amplitude of output pulses as a function of time after the start of the received pulse. Straight line fit gives exponential growth rate of 128 dB s^{-1}. Total growth is $A_m - A_i = 30$ dB (after Helliwell and Katsufrakis, 1974).

maintained over a fairly wide range of amplitudes as long as the input signal is on. As soon as the input signal is shut off growth substantially stops and the frequency begins to change. Sometimes a few dB of exponential growth is observed after the input pulse terminates but usually the growth stops at that point. The details of the phase-locking mechanism are not yet understood.

An important question is whether the magnetosphere must be primed by a triggering signal in order to produce the interactions observed. A number of cases of sudden turn on of the transmitter have been observed in this experiment. They show that the response is immediate, with no buildup time required.

In connection with the two frequency operation of the transmitter it has been found that the emissions triggered at one frequency are frequently cutoff at the other frequency. This is illustrated in Figure 18. In addition, many of the emissions are found

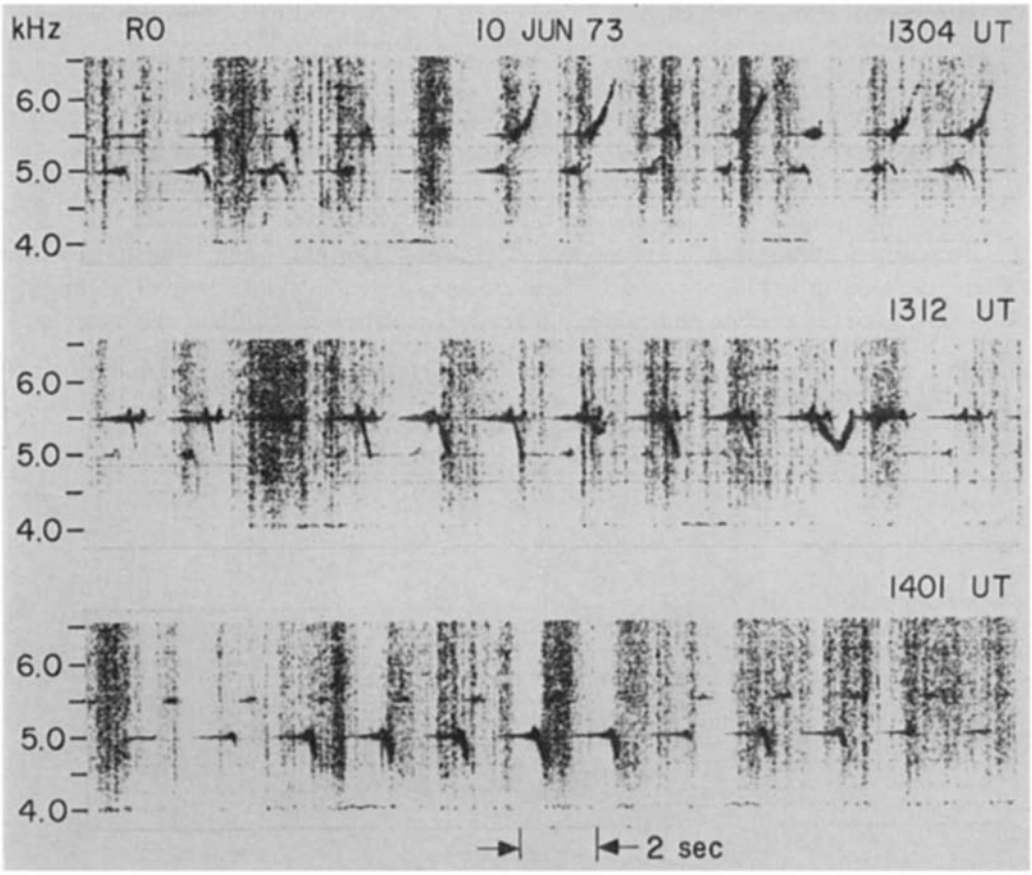

Fig. 18. Alternating one-second transmissions on 5000 and 5500 Hz. Middle panel shows falling tones triggered at 5005 Hz that are cutoff by the weaker signals on 5000 Hz. Triggering on two paths of about 0.4 s separation in time, is frequently present in the middle panel (after Helliwell and Katsufrakis, 1974).

either to terminate or to change slope at power line harmonics. Examples of these power line harmonics are shown in Figure 19. It is even found that some whistlers and emissions are turned on after they cross a harmonic line. On occasion emissions begin at the power line harmonics.

It is suggested that radiation from the Canadian power system enters the magnetosphere and is amplified in much the same way as the signal from the Siple transmitter. These amplified power line harmonics then interact with emissions, affecting their intensity and rate of change of frequency. They may also affect the intensity of whistlers. The mechanism may be connected with the bunching process outlined earlier. The bunching process depends upon the presence of a coherent signal and the addition of another signal of different frequency would alter the phase of the total signal. In addition, the beat between the two signals would produce peaks in total signal that

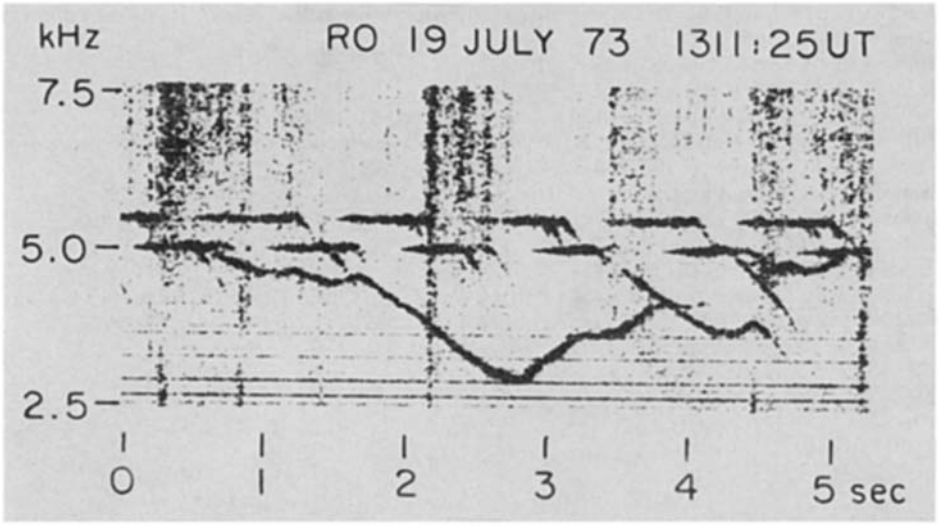

Fig. 19. Hooks triggered at 5.0 kHz show inflections and reversals in slope at power line harmonics, defined by the horizontal lines (after Helliwell and Katsufrakis, 1974).

might trigger an instability of larger amplitude. However, it is too early to draw any conclusions regarding this interesting new phenomenon. The ability of power line harmonics both to terminate and to trigger emissions may account for some of the peculiar properties of natural emissions observed in the past. For example chorus is often limited to a well defined frequency band. The frequencies bounding this band might be power line harmonics.

These experiments open up a new field of magnetospheric study in which the process of wave particle interaction can be studied under controlled conditions. In addition it appears that the wave injection experiment can provide a new tool for studying particle precipitation effects and for modifying the ionosphere and the magnetosphere. It may also be valuable in the study of fundamental plasma instabilities, of interest in fusion devices and astrophysical bodies, such as pulsars. Applications to vlf communications may also be found. The nonlinear effects shown by this experiment have not been explained by any theory currently available in the literature. Attempts to model this process on a computer as described in this paper show some success in explaining the observed observations. The model may therefore provide a new direction for research on nonlinear plasma instabilities.

References

Bell, T. F. and Helliwell, R. A.: 1971, *J. Geophys. Res.* **76**, 8414.
Brice, N. M.: 1964, *J. Geophys. Res.* **69**, 4698.
Carpenter, D. L. and Park, C. G.: 1973, *Rev. Geophys.* **11**, 133.
Edgar, B. C.: 'The Structure of the Magnetosphere as Deduced from Magnetospherically Reflected Whistlers', Tech. Rept. 3438-2, Radioscience Lab., Stanford Electronics Labs., Stanford Univ., Stanford.

Gendrin, R.; 1972, in E. R. Dyer (ed.), *Solar-Terrestrial Physics/1970: Part II*, D. Reidel Publ. Co., Dordrecht-Holland, p. 236.
Helliwell, R. A.: 1967, *J. Geophys. Res.* **72**, 4773.
Helliwell, R. A.: 1969, *Rev. Geophys.* **7**, 281.
Helliwell, R. A. and Crystal, T. L.: 1973, *J. Geophys. Res.* **78**, 7357.
Helliwell, R. A. and Katsufrakis, J. P.: 1974, 'VLF Wave Injection into the Magnetosphere from Siple Station, Antarctica, *J. Geophys. Res.*, submitted 1973.
Helliwell, R. A., Katsufrakis, J. P., and Trimpi, M. L.: 1973, *J. Geophys. Res.* **78**, 4679.
Kimura, I., 1967, *Planetary Space Sci.* **15**, 1427.
Kimura, I.: 1968, *J. Geophys. Res.* **73**, 445.
Liemohn, H. B.: 1967, *J. Geophys. Res.* **72**, 39.
Likhter, Ya. I., Molchanov, O. A., and Chmyrev, V. M.: 1971, *Sov. Phys., JETP Letters* **14**, 325.
Rosenberg, T. J., Helliwell, R. A., and Katsufrakis, J. P.: 1971, *J. Geophys. Res.* **76**, 8445.
Smith, R. L. and Angerami, J. J.: 1968, *J. Geophys. Res.* **73**, 1.